

# TotalSegmentator: robust segmentation of 104 anatomical structures in CT images

Jakob Wasserthal<sup>1</sup> Manfred Meyer<sup>1</sup> Hanns-Christian Breit<sup>1</sup> Joshy Cyriac<sup>1</sup> Shan Yang<sup>1</sup> Martin Seegeroth<sup>1</sup>

## Abstract

In this work we focus on automatic segmentation of multiple anatomical structures in (whole body) CT images. Many segmentation algorithms exist for this task. However, in most cases they suffer from 3 problems: 1. They are difficult to use (the code and data is not publicly available or difficult to use). 2. They do not generalize (often the training dataset was curated to only contain very clean images which do not reflect the image distribution found during clinical routine), 3. The algorithm can only segment one anatomical structure. For more structures several algorithms have to be used which increases the effort required to set up the system. In this work we publish a new dataset and segmentation toolkit which solves all three of these problems: In 1204 CT images we segmented 104 anatomical structures (27 organs, 59 bones, 10 muscles, 8 vessels) covering a majority of relevant classes for most use cases. We show an improved workflow for the creation of ground truth segmentations which speeds up the process by over 10x. The CT images were randomly sampled from clinical routine, thus representing a real world dataset which generalizes to clinical application. The dataset contains a wide range of different pathologies, scanners, sequences and sites. Finally, we train a segmentation algorithm on this new dataset. We call this algorithm TotalSegmentator and make it easily available as a pretrained python pip package (pip install totalsegmentator). Usage is as simple as TotalSegmentator -i ct.nii.gz -o seg and it works well for most CT images. The code is available at <https://github.com/wasserth/TotalSegmentator> and the dataset at <https://doi.org/10.5281/zenodo.6802613>.

<sup>1</sup>Radiology Department, University Hospital Basel, Switzerland. Correspondence to: Jakob Wasserthal <jakob.wasserthal@usb.ch>.

## 1. Introduction

The ever-increasing number of radiological images leads to the need for computer-based evaluation methods. One important building block for the automatic analysis of radiological images is the segmentation of major anatomical structures. There has been a lot of work on segmenting specific anatomical structures, e.g. pancreas (Simpson et al., 2019), spleen (Simpson et al., 2019), colon (Gayathri Devi & Radhakrishnan, 2015), lung (Hofmanninger et al., 2020) and many more. There has also been work on segmenting several anatomical structures in one dataset and model (e.g. multiple organs ((Kavur et al., 2021), (Okada et al., 2012), (Rister et al., 2020), (Norajitra & Maier-Hein, 2017), (Chen et al., 2021)) or multiple vertebrae (Sekuboyina et al., 2021)). However, all of those models only cover a small subset of relevant anatomical structures and train on a dataset which is not representative of a typical clinical population. To the best of our knowledge, this is the first work trying to segment over 100 classes. The closest work is from Chen et al. (Chen et al., 2021) which segments 50 classes. However, they are still missing many classes, the dataset as well as the model is not publically available (the model can only be accessed via uploading data to a web interface) and the dataset is less diverse (the majority of the training data comes from the same scanner and uses the same CT sequence).

With our approach we solve all three of these problems:

1. Our model segments a wide range of anatomical structures.
2. Our model robustly works on clinical data since it was trained on a large clinical dataset.
3. Our model as well as the training data is publicly available and very easy to use.

## 2. Methods

### 2.1. Data selection

The following dataset was collected to train our model: Over the timespan of the last 10 years, we randomly sampled CT images from our PACS. Only images from patients with a general research consent were used. CT images of legs and

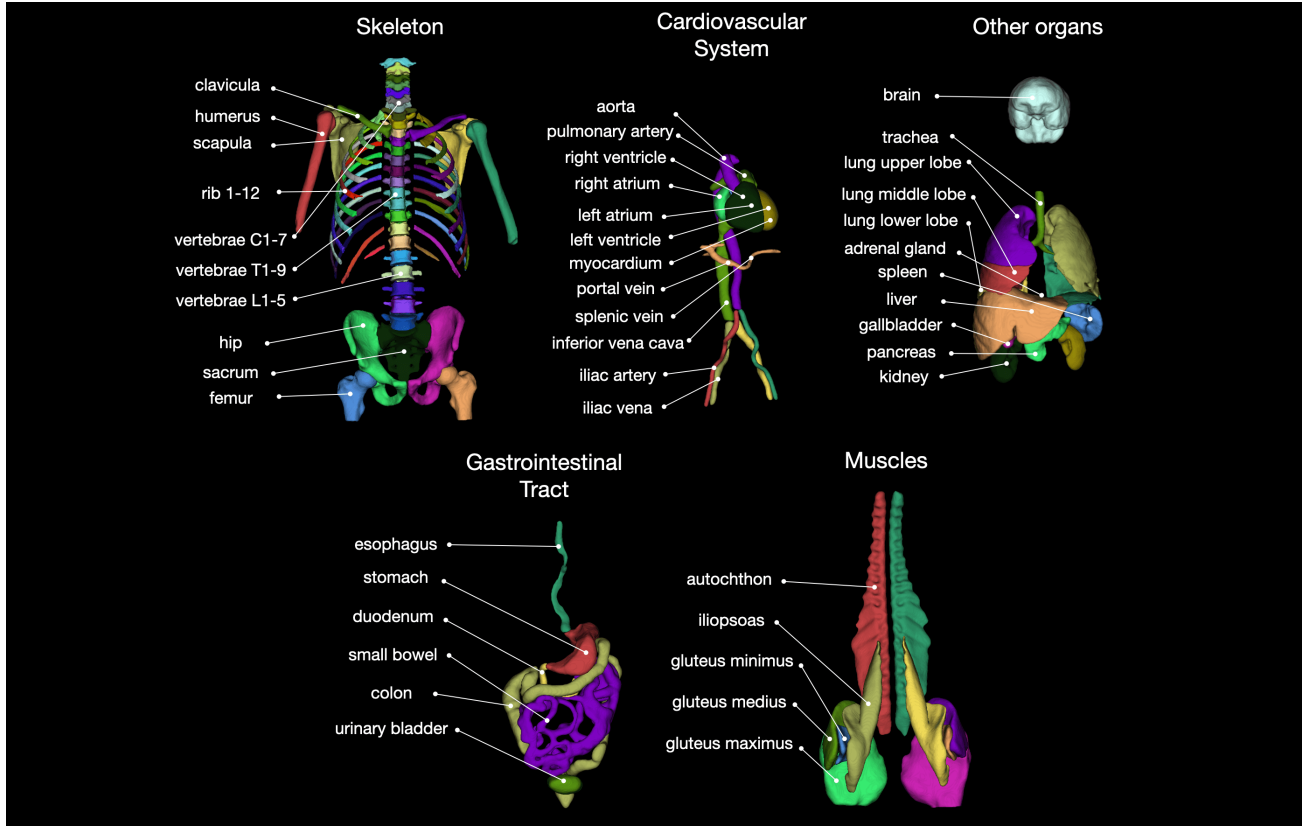


Figure 1. Overview of all 104 anatomical structures which can be segmented by the TotalSegmentator.

hands were excluded. We also sampled the CT series of each examination randomly. Thus, the dataset contains CT images with different sequences (native, arterial, portal venous, late phase, dual energy), with and without contrast agent, with different bulb voltages, with different slice thicknesses and resolution and with different kernels (soft tissue kernel, bone kernel). If the human expert annotator was unsure how to segment certain structures because of high ambiguity (e.g. structures highly distorted by pathologies), the examination was excluded (40 subjects). The final dataset contains 1204 images. Figure 2 shows the distribution of CT image types, age distribution and distribution over sites (each site is anonymised with a letter) where the images were acquired.

## 2.2. Data annotation

Based on clinical experience 104 anatomical structures, the classes of our model, were identified for segmentation (see figure 1 for a graphical overview and supplementary materials figure 11 for a complete list). Complete manual segmentation for one class takes roughly 10 min. Based on this time for manual segmentation of 104 classes in 1204

subjects it would have taken one person over 10 years to complete the segmentation (assuming the person is working 8 h per day and 5 days a week). This would not be feasible. We used the following approach to speed up the process by several orders of magnitude:

### 1. Using existing models

If for a certain structure an existing model was publicly available, this model was used to create a first segmentation which was then further refined manually if necessary. Given the high variability of our dataset a further refinement was often necessary. Supplementary materials S1 shows a complete list of the used models. This gave us a first segmentation for 68 classes. For the remaining 36 classes, manual segmentation was necessary. Refinement of segmentations as well as manual segmentation was supervised by a board-certified radiologist.

### 2. Transfer of segmentations between CTs with and without contrast agent

To be able to segment the different heart subparts (left/right atrium, left/right ventricle, myocardium, pulmonary artery) on all different CT series (also without contrast agent), the following approach was taken: An inhouse dataset was

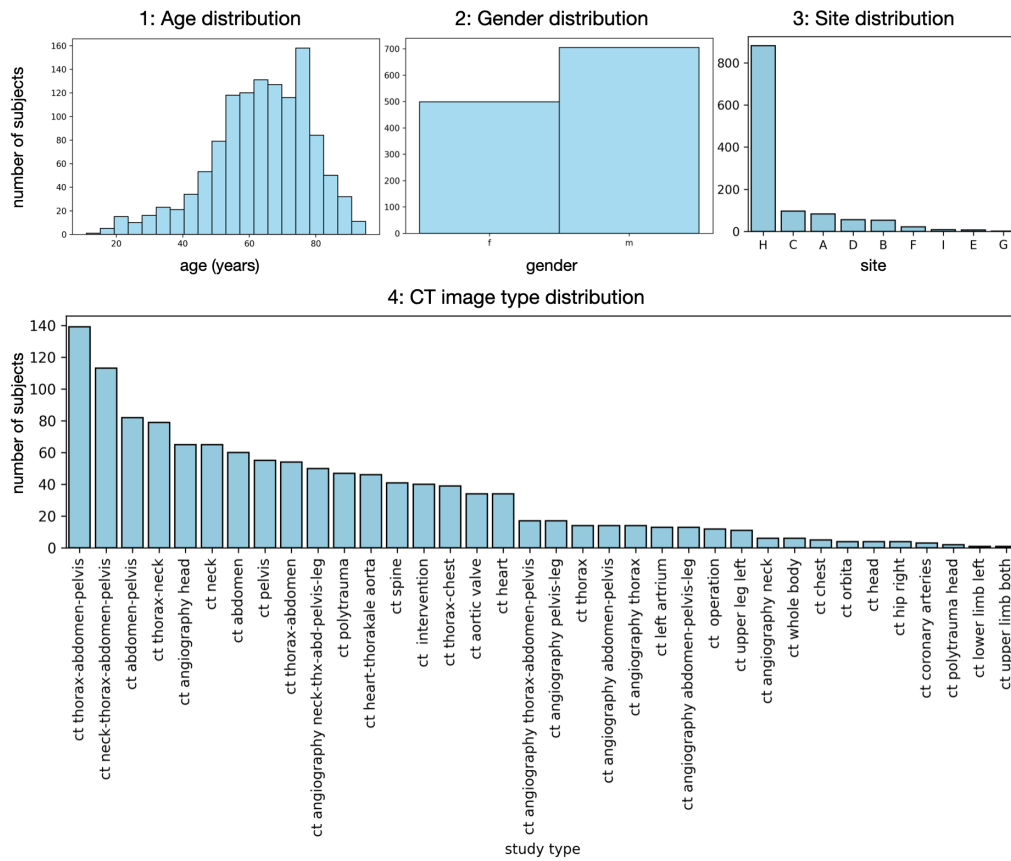


Figure 2. Overview of characteristics of the training dataset. 1: Age distribution, 2: gender distribution, 3: Site (where the images were acquired) distribution, 4: CT image type distribution.

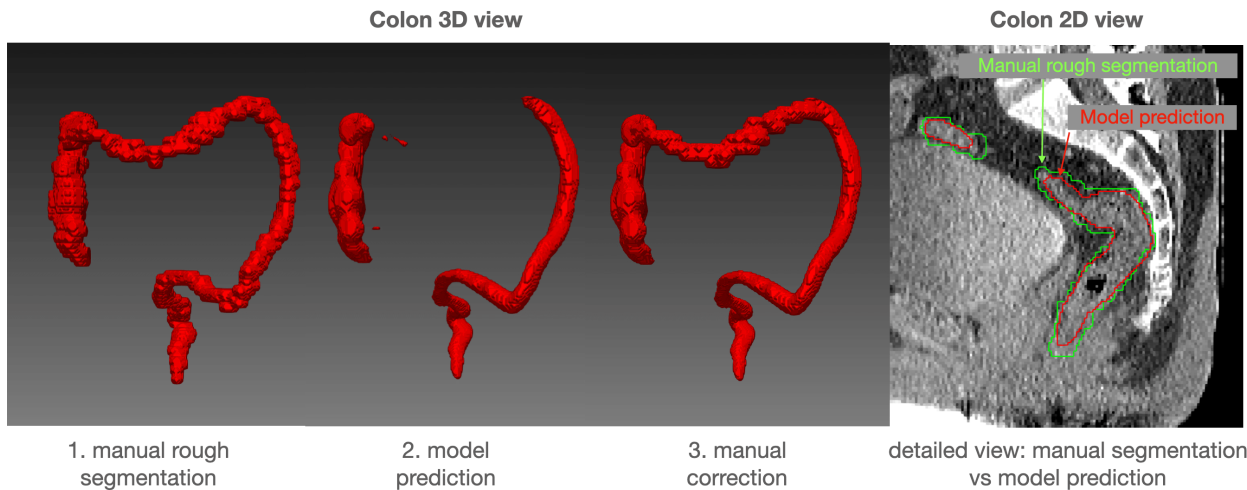


Figure 3. Example of steps from ground truth creation: It can be seen how the model generates smooth predictions from rough ground truth segmentations and how errors in the model predictions are corrected.

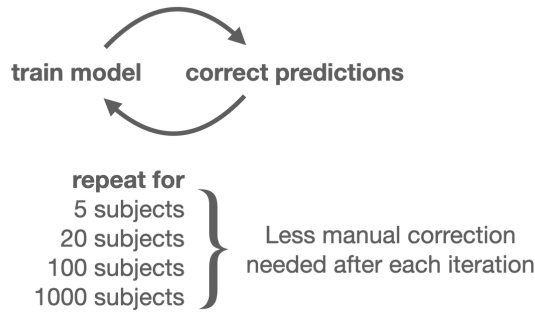


Figure 4. Overview of the active learning approach for manual segmentation: In a first step 5 subjects need to be labeled completely manually. Then a model is trained and only the model predictions are corrected. As soon as more data is labeled, the model is retrained, reducing the amount of manual corrections required.

available with ground truth segmentations of the heart subparts on CT images with contrast agent. For each image with contrast agent also a native CT image without contrast agent was available. Since this image was from the same examination it was well aligned with the contrast agent image. So, we transferred the segmentation to the CT images without contrast agent and trained a U-Net (Ronneberger et al., 2015) on images with and without contrast agent. This model was then used to predict the heart subparts in our dataset, resulting in very accurate segmentations of the heart subparts in all kinds of CT sequences.

### 3. Improved segmentation workflow

To speedup manual segmentation we used the Nora imaging platform (Anastasopoulos et al., 2017). Compared to traditional tools like MITK (Wolf et al., 2005), Nora provides the following advantages: First, subjects do not have to be loaded individually, instead Nora provides a list of all subjects. Second, segmentation masks do not have to be created and saved individually for each image, but whenever you change the subject in Nora, the correct masks are created, named and saved automatically. Third, the autoloading as well as the view (e.g. the intensity window) can be configured for each project individually. Thus, it took us only 17 s in Nora to load the case, create a segmentation mask and save the segmentation mask, whereas with MITK this procedure took us 45 s. Forth, an even higher speedup is achieved by doing rough segmentations instead of pixel perfect segmentations. Those rough segmentations were preliminary and not sufficient for the final result. However, the U-Net is good at learning good segmentations from rough segmentations. The errors in the rough segmentations are rather random across subjects (no systematic error) and therefore

the U-Net learns to ignore the random part of the segmentation and keeps the consistent part which aligns pretty well with the anatomical structure. Figure 3 shows how the U-Net produces a smooth segmentation from the rough input. Fifth, since rough segmentations are sufficient we used a pencil for segmentation which draws through 3 slices at the same time, providing another speedup. Exemplary, detailed segmentation of the urinary bladder takes 10 min whereas rough segmentation only takes 1 min 25 s and the U-Net produces accurate results also from these rough segmentations. Overall, using a traditional segmentation approach takes 45 s for loading/saving and 10 min for segmentation whereas using our approach it only takes 17 s for loading/saving and 1 min 25 s for segmentation. Thus, this process could be made 7x faster.

### 4. Active learning

For further speedup, we used an active learning approach: After finishing manual segmentation of the first 5 subjects, a U-Net was trained and only its predictions were corrected. The U-Net was then retrained again after 20 subjects, 100 subjects and 1000 subjects. After each iteration, less manual correction was necessary.

### 5. 3D preview for quality control

Another great speedup was achieved by using 3D renderings (using the python fury library (Garyfallidis et al., 2021)) of the masks to spot errors. After 1 or 2 iterations of the active learning the predictions of most segmentations did not need further refinement. However, it takes a lot of time to load all masks and scroll through all slices to check if they are fine or need correction. This task can be greatly accelerated by generating one PNG image with a 3D rendering of all the 104 masks. We tested this approach on many subjects and it turns out that if a mask has errors you can typically spot it in the 3D rendering (see figure 9). Moreover, the loading of the PNG image is instant, instead of several minutes for loading 104 masks. With this approach, 104 masks can be checked for errors within several seconds instead of several minutes with a traditional approach. When evaluating segmentations only based on 3D renderings minor errors can be missed. However, for evaluation of major anatomical structures (in contrast to e.g. small lung nodules) errors which can not be seen in the 3D rendering are very rare. And also if evaluating segmentations slice by slice errors can easily be missed since expert raters tend to become negligent when looking at thousands of slices. In several cases we spotted errors in the 3D rendering which were missed by a previous slice by slice evaluation.

With our approach, we managed to finish the segmentation in roughly 8 weeks with 1 person working on it on average. Compared to the 10 years for complete manual segmentation this is a 65x speedup.

In many cases the quality of the segmentations is also better

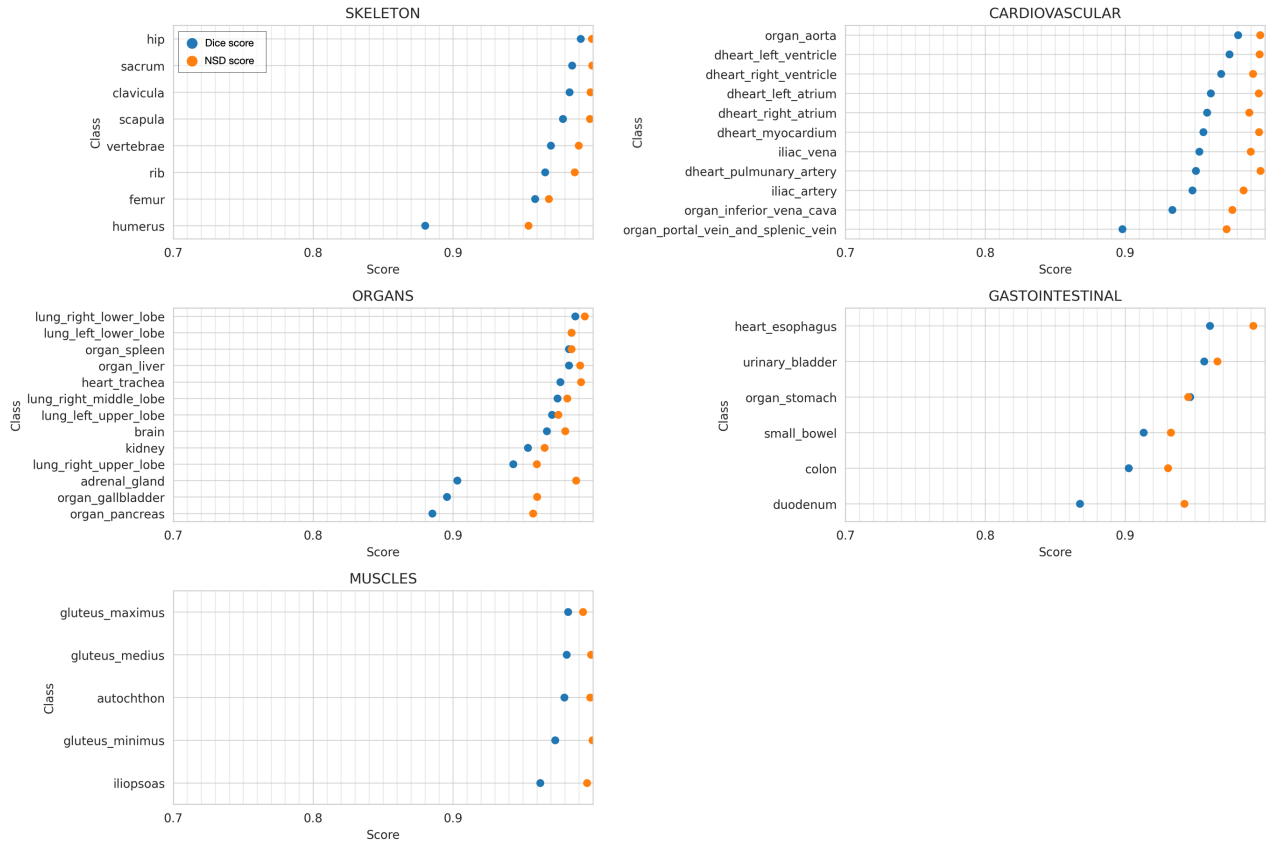


Figure 5. Results of high resolution model per class (similar classes e.g. ribs or left/right of the same class are grouped together).

using our approach, than using a completely manual segmentation: When an expert is doing a manual segmentation it has to be done slice by slice. In consequence those segmentations tend to be slightly inconsistent between slices as can be seen when looking at it from another orientation or in a 3D rendering. Moreover, whenever an expert is working on this for 8 h per day he tends to become bored and therefore starts to do the segmentation less precisely. By using generated segmentations and only correcting the mistakes, our segmentations avoid these problems.

The face region was also segmented. In the end all faces had to be blurred for anonymization. Moreover, for further anonymization a random number between -2 and +2 was added to the age of each subject.

### 2.3. Model

As model we use the nnU-Net (Isensee et al., 2021; 2018; 2020). This is a U-Net implementation which automatically configures all hyperparameters based on the dataset characteristics. This approach has been shown to deliver state of the art results while being very easy to apply. We

did 2 adaptations to the default nnU-Net settings: We removed mirroring from the data augmentation because with mirroring the model was not able to properly distinguish between left and right bones. Moreover, the number of training epochs was increased from the default of 1000 to 4000 given the large size of the dataset. For the low resolution model it was increased even further to 8000 epochs since training took longer given the high number of classes in one model (104 output classes for the low resolution model). From the different nnU-Net model types we only used the 3D full resolution model. All images were resampled to 1.5 mm isotropic resolution. On this resolution, the segmentation was done and the model was trained. In general, the nnU-Net can be trained to predict all 104 classes at the same time. This required a lot of memory because the nnU-Net has to store the softmax predictions of all classes at the same time resulting in a huge image of dimensions Width x Height x Depth x Number\_of\_classes. Instead the 104 classes were split into 5 parts with 21 classes each and for each part one nnU-Net was trained. However, for large images this still required a lot of RAM and GPU memory. Many users will not have such a machine. Therefore, we trained a model



on data resampled to 3 mm isotropic resolution. Given the lower resolution it was possible to train all 104 classes in one model, achieving faster runtime. If the user chooses the flag “-fast” in our toolkit then this 3 mm model will be used. When performing larger studies on many thousand subjects the “-fast” option can be helpful to make processing of so many subjects feasible.

## 2.4. Evaluation

The dataset of 1204 subjects was randomly split into 1082 training subjects (89.9%), 57 validation subjects (4.7%) and 65 subjects for final testing (5.4%). All results are reported on the test set. As metric, we used the Dice score as well as the normalized surface distance (NSD) (using the function “compute\_surface\_dice\_at\_tolerance” from <https://github.com/deepmind/surface-distance>). For many applications (e.g. localisation of a certain organ) it is not necessary to precisely segment the organ boundary as long as the overall segmentation is correct. For this, the surface distance is a good measure. We set the threshold to 3 mm. This means that all areas of the segmentation surface are counted as correct if they are within 3 mm of the ground truth segmentation surface. Just as the Dice score, the NSD scores ranges between 0 and 1 with 1 being the best score. Moreover, the Dice score is biased towards big classes: the inner voxels are normally easier to predict than the border voxels, but in the Dice score they are equally weighted. In big classes, the ratio of inner voxels to border voxels is typically high and therefore the Dice score tends to be better. In contrast, the normalized surface distance with a high threshold of 3 mm is biased towards small classes: For thin structures like the iliac arteries almost the entire structure is within the 3 mm threshold. So the segmentation could miss parts of the class and still be counted as correct because it is within the 3 mm threshold. Therefore, looking at both metrics is important for proper evaluation. For each class in each subject the respective metric is calculated and then the mean is taken across all classes and subjects (micro-average).

As additional evaluation we compared our model to a nnU-Net trained on the dataset from the “Multi-Atlas Labeling Beyond the Cranial Vault Challenge” <https://doi.org/10.7303/syn3193805> (nnU-Net Task 17). With this model we predicted our test set and compared the results to our model. This dataset only provides labels for 13 classes. So the comparison is limited to those.

## 3. Results

### 3.1. Overall results

Our two models (one on 1.5 mm resolution and another one on 3 mm), have good accuracy regarding the segmentation.

Figure 6 shows the mean results over all classes for both models. The model trained on CTs with a slice thickness of 1.5 mm shows high accuracy: both Dice as well as NSD are over 0.96. For the 3 mm model the Dice score is reduced to 0.85, while the NSD is over 0.96 because the minor inaccuracies introduced by the lower resolution are still within the bounds of the 3 mm resolution. Thus it follows that the 3 mm model still delivers correct results, but the borders are less precise. For many applications this is acceptable.

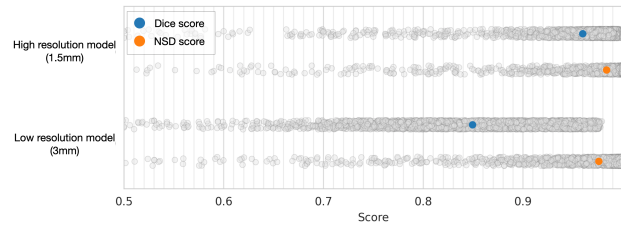


Figure 6. Results (Dice score and normalized surface distance [NSD score]) of high resolution model and low resolution model on all classes (bar shows the 95% confidence interval. It is so tight, that it is completely covered by the dot).

### 3.2. Results per class

Figure 5 shows the results for all classes independently. We grouped similar classes (e.g. left and right, all ribs, all vertebrae) for better readability. Results vary between 0.87 and 1.0.

### 3.3. Comparison to other model

Figure 7 shows the comparison of our high resolution model (1.5mm) to the nnU-Net trained on the data from the “Multi-Atlas Labeling Beyond the Cranial Vault Challenge”. Our model achieves a higher dice and a higher NSD score.

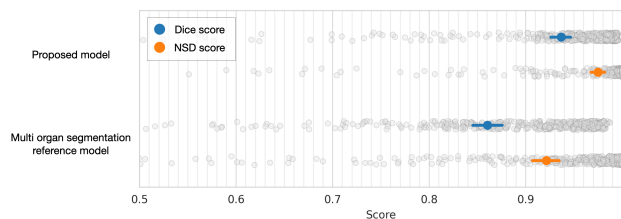


Figure 7. Comparison of proposed model (high resolution model) with publicly available multi organ segmentation model (bar shows the 95% confidence interval).

### 3.4. Runtime

Table 8 shows an overview of the runtime, RAM requirements as well as GPU memory requirements of the high resolution (1.5 mm) and the low resolution model (3 mm) on three different CT images with different dimensions.: A small image of only abdomen with shape 512 x 512 x 280 voxels, a medium image of the thorax and abdomen with shape 512x512x458 voxels and a large image from head to knee with shape 512x512x824 voxels. The runtime was measured on a local workstation with a NVidia GeForce RTX 3090 GPU.

Image Size	1.5mm model			3mm model		
	Runtime	RAM	GPU Mem	Runtime	RAM	GPU Mem
Small (512x512x280)	1min 17s	7.6GB	6.1GB	34s	7.4GB	5.2GB
Medium (512x512x458)	2min 49s	10.6GB	8.5GB	53s	8.4GB	7.4GB
Large (512x512x824)	3min 32s	11.8GB	11.4GB	1min 23s	10.6GB	7.5GB

Figure 8. Overview of runtime, RAM requirements as well as GPU memory requirements of the high resolution (1.5mm) and the low resolution model (3mm) on three different CT images: A small image of only abdomen with shape 512x512x280 voxels, a medium image of the thorax and abdomen with shape 512x512x458 voxels and a large image from head to knee with shape 512x512x824 voxels.

### 3.5. Typical failure cases

For all classes our model consistently produces highly accurate results. Given the high diversity of the dataset, this demonstrates the robustness of our model. However, there are a few typical failure cases which occur in roughly 15% of the subjects. Those can be seen in figure 9. Being aware of those can be helpful when using the segmentations of the affected classes.

### 3.6. Application example

As one example of what our model can be used for, we show an aging study: How does the density (in Hounsfield units [HU]) as well as the volume of different anatomical structures change over the lifespan. For this, we collected a dataset of 4102 whole body CTs performed in case of a polytrauma (for age and gender distribution see supplementary materials figure 12). Those images were acquired from patients coming to the hospital because of an accident. Normally, only a small subset of the anatomical structure is damaged by the accident. Therefore, thanks to the high number of included cases, on average, this dataset presents a random sample from patients aged 18 to 100 years. As an example, we show the results for 3 anatomical structures: liver, left atrium of the heart and hip (see figure 10). For

the liver we can see that up to the age of 50 it is growing in volume and then shrinking. The density of the liver is following an inverse trajectory. It is falling up to the age of 60 and then rising again. For the left atrium it can be seen that over the entire lifespan it is rising in volume and density. For the hip we can see that it is growing up to roughly the age of 60 and then remaining constant in size. The bone density however is constantly falling over the lifespan. The same analysis can easily be done for all of the 104 classes.

## 4. Conclusion

As we have shown our model produces accurate segmentation across a very diverse dataset which is directly sampled from clinical routine. We hope that many researchers find our model helpful for their use cases. We made it openly available on github (<https://github.com/wasserth/TotalSegmentator>) and it can be easily installed via pip

```
pip install totalsegmentator
```

and easily used

```
TotalSegmentator -i ct.nii.gz -o seg_dir
```

Please note that a NVidia GPU with CUDA support is required to run the code. For people without a GPU we provide an online tool to upload images for segmentation: [www.totalsegmentator.com](http://www.totalsegmentator.com).

We also made our dataset of 1204 subjects with 104 ground truth segmentations publicly available: <https://doi.org/10.5281/zenodo.6802613>. In future work we are planning to further extend the number of classes. Currently we are working on adding more vessel segmentations.

## Acknowledgements

We thank all our colleagues at University Hospital Basel who contributed to this work with ideas and comments.

## References

- Anastasopoulos, C., Reisert, M., and Kellner, E. “Nora Imaging”: A Web-Based Platform for Medical Imaging. In *Neuropediatrics*, volume 48, pp. P26. Georg Thieme Verlag KG, April 2017. doi: 10.1055/s-0037-1602977. URL <http://www.thieme-connect.de/DOI/DOI?10.1055/s-0037-1602977>. ISSN: 0174-304X, 1439-1899 Issue: S 01 Journal Abbreviation: Neuropediatrics.
- Chen, X., Sun, S., Bai, N., Han, K., Liu, Q., Yao, S., Tang, H., Zhang, C., Lu, Z., Huang, Q., Zhao, G., Xu, Y., Chen, T., Xie, X., and Liu, Y. A deep learning-based

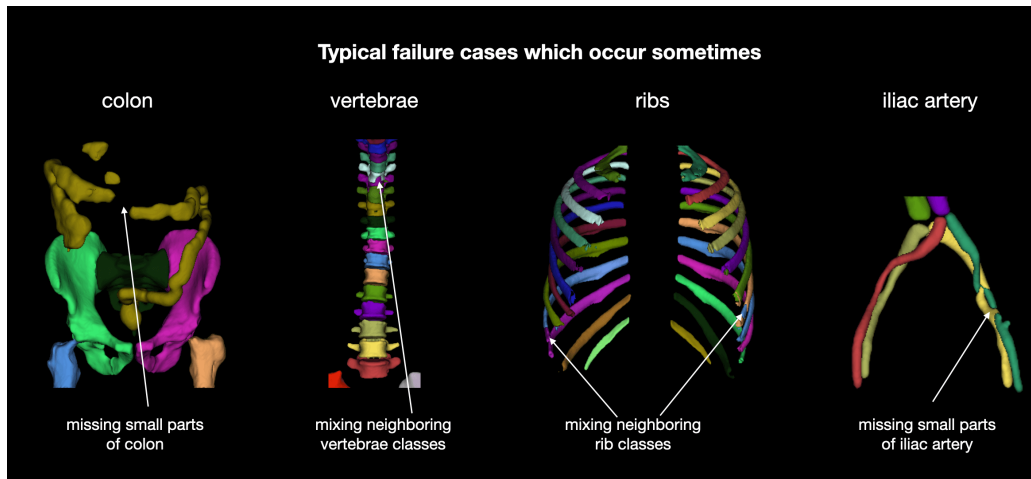


Figure 9. Overview of typical failure cases of the proposed model. Users should be aware that these problems can occur in roughly 15% of the subjects.

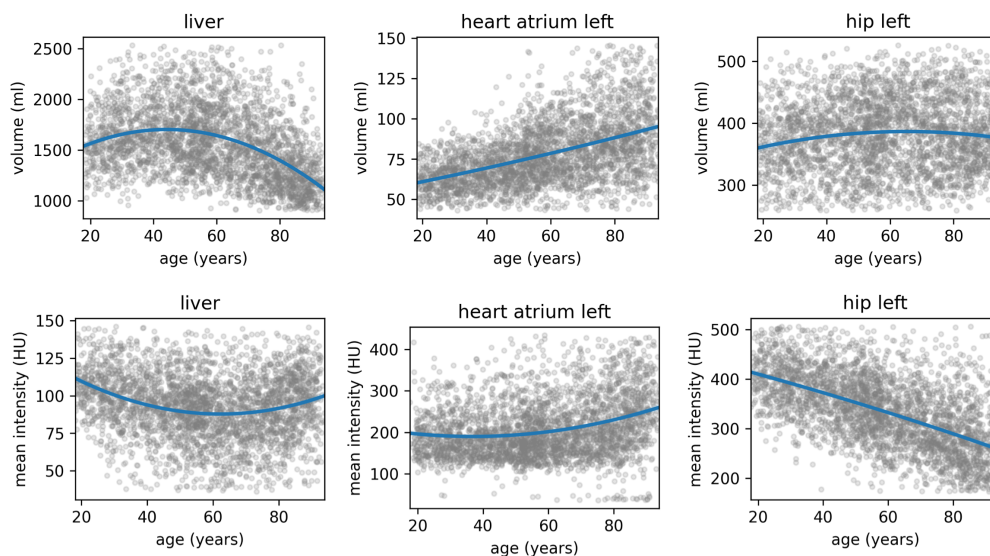


Figure 10. Mean density (in HU) and volume of three exemplary classes over the entire lifespan of a polytrauma cohort of 4102 subjects. It can be seen how both measures significantly change over the lifespan. (Blue line: fit of quadratic model)

auto-segmentation system for organs-at-risk on whole-body computed tomography images for radiation therapy. *Radiotherapy and Oncology*, 160:175–184, July 2021. ISSN 0167-8140. doi: 10.1016/j.radonc.2021.04.019. URL <https://www.sciencedirect.com/science/article/pii/S0167814021062174>.

Garyfallidis, E., Koudoro, S., Guaje, J., Côté, M.-A., Biswas, S., Reagan, D., Anousheh, N., Silva, F., Fox, G., and Contributors, F. FURY: advanced scientific visualization. *Journal of Open Source Software*, 6 (64):3384, August 2021. ISSN 2475-9066. doi:

10.21105/joss.03384. URL <https://joss.theoj.org/papers/10.21105/joss.03384>.

Gayathri Devi, K. and Radhakrishnan, R. Automatic Segmentation of Colon in 3D CT Images and Removal of Opacified Fluid Using Cascade Feed Forward Neural Network. *Computational and Mathematical Methods in Medicine*, 2015:670739, 2015. ISSN 1748-670X. doi: 10.1155/2015/670739. URL <https://www.ncbi.nlm.nih.gov/pmc/articles/PMC4369940/>.

Hofmanninger, J., Prayer, F., Pan, J., Röhrich, S., Prosch, H., and Langs, G. Automatic lung segmentation in rou-



- tine imaging is primarily a data diversity problem, not a methodology problem. *European Radiology Experimental*, 4(1):50, August 2020. ISSN 2509-9280. doi: 10.1186/s41747-020-00173-2. URL <https://doi.org/10.1186/s41747-020-00173-2>.
- Isensee, F., Petersen, J., Klein, A., Zimmerer, D., Jaeger, P. F., Kohl, S., Wasserthal, J., Koehler, G., Norajitra, T., Wirkert, S., and Maier-Hein, K. H. nnU-Net: Self-adapting Framework for U-Net-Based Medical Image Segmentation, September 2018. URL <http://arxiv.org/abs/1809.10486>. arXiv:1809.10486 [cs].
- Isensee, F., Jäger, P., Wasserthal, J., Zimmerer, D., Petersen, J., Kohl, S., Schock, J., Klein, A., Roß, T., Wirkert, S., Neher, P., Dinkelacker, S., Köhler, G., and Maier-Hein, K. batchgenerators - a python framework for data augmentation, January 2020. URL <https://zenodo.org/record/3632567>.
- Isensee, F., Jaeger, P. F., Kohl, S. A. A., Petersen, J., and Maier-Hein, K. H. nnU-Net: a self-configuring method for deep learning-based biomedical image segmentation. *Nature Methods*, 18(2):203–211, February 2021. ISSN 1548-7105. doi: 10.1038/s41592-020-01008-z.
- Kavur, A. E., Gezer, N. S., Barış, M., Aslan, S., Conze, P.-H., Groza, V., Pham, D. D., Chatterjee, S., Ernst, P., Özkan, S., Baydar, B., Lachinov, D., Han, S., Pauli, J., Isensee, F., Perkonigg, M., Sathish, R., Rajan, R., Sheet, D., Dovletov, G., Speck, O., Nürnberger, A., Maier-Hein, K. H., Akar, G. B., Ünal, G., Dicle, O., and Selver, M. A. CHAOS Challenge – Combined (CT-MR) Healthy Abdominal Organ Segmentation. *Medical Image Analysis*, 69:101950, April 2021. ISSN 13618415. doi: 10.1016/j.media.2020.101950. URL <http://arxiv.org/abs/2001.06535>. arXiv:2001.06535 [cs, eess].
- Norajitra, T. and Maier-Hein, K. H. 3D Statistical Shape Models Incorporating Landmark-Wise Random Regression Forests for Omni-Directional Landmark Detection. *IEEE transactions on medical imaging*, 36(1):155–168, January 2017. ISSN 1558-254X. doi: 10.1109/TMI.2016.2600502.
- Okada, T., Linguraru, M. G., Hori, M., Suzuki, Y., Summers, R. M., Tomiyama, N., and Sato, Y. Multi-Organ Segmentation in Abdominal CT Images. *Conference proceedings : ... Annual International Conference of the IEEE Engineering in Medicine and Biology Society. IEEE Engineering in Medicine and Biology Society. Conference*, 2012:10.1109/EMBC.2012.6346840, 2012. ISSN 1557-170X. doi: 10.1109/EMBC.2012.6346840. URL <https://www.ncbi.nlm.nih.gov/pmc/articles/PMC3855338/>.
- Rister, B., Yi, D., Shivakumar, K., Nobashi, T., and Rubin, D. L. CT-ORG, a new dataset for multiple organ segmentation in computed tomography. *Scientific Data*, 7(1):381, November 2020. ISSN 2052-4463. doi: 10.1038/s41597-020-00715-8. URL <https://www.nature.com/articles/s41597-020-00715-8>. Number: 1 Publisher: Nature Publishing Group.
- Ronneberger, O., Fischer, P., and Brox, T. U-Net: Convolutional Networks for Biomedical Image Segmentation. In Navab, N., Hornegger, J., Wells, W. M., and Frangi, A. F. (eds.), *Medical Image Computing and Computer-Assisted Intervention – MICCAI 2015*, Lecture Notes in Computer Science, pp. 234–241, Cham, 2015. Springer International Publishing. ISBN 978-3-319-24574-4. doi: 10.1007/978-3-319-24574-4\_28.
- Sekuboyina, A., Husseini, M. E., Bayat, A., Löffler, M., Liebl, H., Li, H., Tetteh, G., Kukačka, J., Payer, C., Štern, D., Urschler, M., Chen, M., Cheng, D., Lessmann, N., Hu, Y., Wang, T., Yang, D., Xu, D., Ambellan, F., Amiranashvili, T., Ehlke, M., Lamecker, H., Lehnert, S., Lirio, M., Olaguer, N. P. d., Ramm, H., Sahu, M., Tack, A., Zachow, S., Jiang, T., Ma, X., Angerman, C., Wang, X., Brown, K., Kirszenberg, A., Puybareau, E., Chen, D., Bai, Y., Rapazzo, B. H., Yeah, T., Zhang, A., Xu, S., Hou, F., He, Z., Zeng, C., Xiangshang, Z., Liming, X., Netherton, T. J., Mummie, R. P., Court, L. E., Huang, Z., He, C., Wang, L.-W., Ling, S. H., Huynh, L. D., Boutry, N., Jakubicek, R., Chmelik, J., Mulay, S., Sivaprakasam, M., Paetzold, J. C., Shit, S., Ezhov, I., Wiestler, B., Glocker, B., Valentinitzsch, A., Rempfler, M., Menze, B. H., and Kirschke, J. S. VerSe: A Vertebrae labelling and segmentation benchmark for multi-detector CT images. *Medical Image Analysis*, 73:102166, October 2021. ISSN 1361-8415. doi: 10.1016/j.media.2021.102166. URL <https://www.sciencedirect.com/science/article/pii/S1361841521002127>.
- Simpson, A. L., Antonelli, M., Bakas, S., Bilello, M., Farhani, K., van Ginneken, B., Kopp-Schneider, A., Landman, B. A., Litjens, G., Menze, B., Ronneberger, O., Summers, R. M., Bilic, P., Christ, P. F., Do, R. K. G., Gollub, M., Golia-Pernicka, J., Heckers, S. H., Jarnagin, W. R., McHugo, M. K., Napel, S., Vorontsov, E., Maier-Hein, L., and Cardoso, M. J. A large annotated medical image dataset for the development and evaluation of segmentation algorithms, February 2019. URL <http://arxiv.org/abs/1902.09063>. arXiv:1902.09063 [cs, eess].
- Wolf, I., Vetter, M., Wegner, I., Böttger, T., Nolden, M., Schöbinger, M., Hastenteufel, M., Kunert, T., and Meinzer, H.-P. The Medical Imaging Interaction Toolkit. *Medical Image Analysis*, 9(6):594–604, December 2005. ISSN 1361-8415. doi: 10.1016/j.media.2005.04.

005. URL <https://www.sciencedirect.com/science/article/pii/S1361841505000344>.

## Supplementary materials

### A. List of pretrained models used during data annotation

- **Name:** Multi-Atlas Labeling Beyond the Cranial Vault - Abdomen (nnU-Net Task 17) (<https://doi.org/10.7303/syn3193805>)  
**Classes:** spleen, kidney left/right, gallbladder, esophagus, liver, stomach, aorta, inferior vena cava, portal vein and splenic vein, pancreas, adrenal gland left/right
- **Name:** RibFrac 2020 Challenge <https://ribfrac.grand-challenge.org/dataset/>  
**Classes:** 24 ribs (the dataset only provides segmentations of all ribs; with postprocessing we split this into instance segmentations for each rib).
- **Name:** Large Scale Vertebrae Segmentation Challenge <https://github.com/anjany/verse>  
**Classes:** 25 vertebrae
- **Name:** Johof Lung Segmentation <https://github.com/JoHof/lungmask>  
**Classes:** 5 lung lobes
- **Name:** SegTHOR: Segmentation of THoracic Organs at Risk in CT images (nnU-Net Task 55) <https://competitions.codalab.org/competitions/21145>  
**Classes:** aorta, esophagus, heart, trachea

### B. Results for all classes

### C. CT polytrauma dataset characterisation

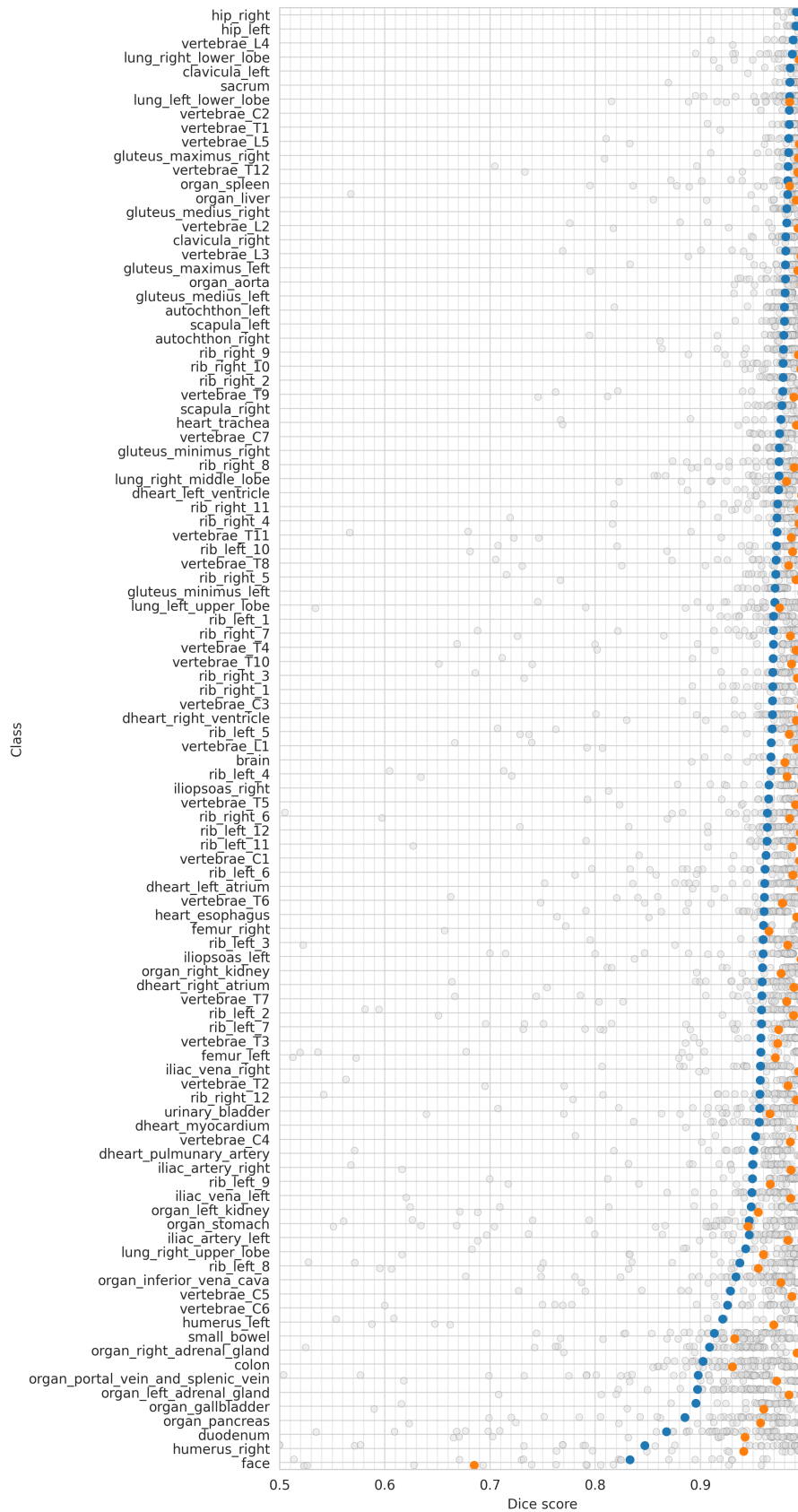


Figure 11. Results for all 104 classes for proposed high resolution model. (Blue: Dice score, Orange: NSD score).

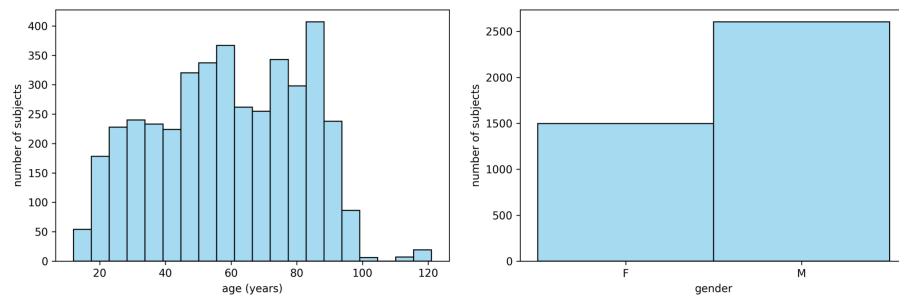


Figure 12. Overview of characteristics of the polytrauma dataset used in the application example. 1: Age distribution, 2: gender distribution.